IOP Publishing Journal of Physics: Condensed Matter
J. Phys.: Condens. Matter **36** (2024) 315504 (10pp) https://doi.org/10.1088/1361-648X/ad4226

Terahertz magneto-optical response in ferromagnetic Fe–Co–Al alloys

Ming Lei[1,*] **and Sinisa Coh**[2]

[1] Chemical and Environmental Engineering, University of California Riverside, Riverside, CA 92521, United States of America
[2] Materials Science and Mechanical Engineering, University of California Riverside, Riverside, CA 92521, United States of America

E-mail: mlei012@ucr.edu

Received 4 October 2023, revised 10 April 2024
Accepted for publication 23 April 2024
Published 9 May 2024

Abstract

We study the magneto-optical properties of Fe–Co–Al ordered alloys in the terahertz range of frequencies. Using the standard Kubo-based approach to compute intrinsic part of the $\sigma_{xy}(\omega)$ we find a strong dependence of σ_{xy} on ω in the terahertz range. For example, we find that below 10 THz Co_3Al has nearly constant σ_{xy} and that above 10 THz it is reduced by about 50 times. Furthermore, we find a strong dependence of σ_{xy} on the chemical composition. For example, we find that the addition of Al to Fe changes the sign of σ_{xy}, while the addition of Co to Fe leads to a nonmonotonic dependence of σ_{xy} on Co concentration.

Supplementary material for this article is available online

Keywords: magneto-optical properties, terahertz, quantum espresso, spin–orbit interaction

1. Introduction

A magnet with a cubic crystal structure and magnetization pointing along the z-axis has a non-zero off-diagonal component of the optical conductivity, $\sigma_{xy}(\omega)$. This contribution to the conductivity occurs because magnetic order in such a system breaks time-reversal symmetry. The breaking of the time-reversal symmetry is propagated to the electronic degrees of freedom by the spin–orbit interaction. Therefore, the magnitude of $\sigma_{xy}(\omega)$ is dictated by the spin–orbit interaction strength [1]. Presence of off-diagonal conductivity σ_{xy}, and thus in-directly the presence of magnetic order, can be detected optically by comparing the polarization of light incident to, and reflected from, the surface of a magnet. This occurs for example in the so-called magneto-optical Kerr effect (MOKE) [2]. Opposite is also true. If one changes the magnetization direction along the z-axis,

$$M_z \rightarrow -M_z,$$

this will result in,

$$\sigma_{xy} \rightarrow -\sigma_{xy}.$$

Therefore, one can use the direction of magnetization to control the way in which light reflects from a surface of a magnet. This effect has been used in memory storage devices [3, 4] and in the creation of tunable photonic materials [5, 6].

At zero frequency, the static conductivity $\sigma_{xy}(\omega = 0)$ produces the anomalous Hall effect (AHE). In materials with very few impurities, so that the diagonal conductivity σ_{xx} is above 10^6 $(\Omega\ \mathrm{cm})^{-1}$, the dominant contribution to AHE originates from the scattering of electrons from the impurities. On the other hand, somewhat paradoxically, in materials with a moderate amount of impurities, with diagonal conductivity around 10^4–10^6 $(\Omega\ \mathrm{cm})^{-1}$, the dominant contribution to AHE is intrinsic, independent of the number of impurities [1]. The intrinsic contribution to AHE is given by the integral of the Berry curvature over the occupied states [7]. However, in the dynamic case, the $\sigma_{xy}(\omega \neq 0)$ can no longer be written as a sum over the Berry curvature, instead it needs to be computed from the Kubo-like sum over empty states, as in [8–11].

* Author to whom any correspondence should be addressed.

Nevertheless, we expect that for small enough ω the intrinsic contribution still dominates $\sigma_{xy}(\omega)$, which is consistent with findings in [12].

There are many calculations of static intrinsic AHC in the literature. For example, Yao *et al* [13] calculated the AHC of ferromagnetic bcc Fe, and the calculated σ_{xy} at zero frequency is 751 $(\Omega\ \mathrm{cm})^{-1}$. Wang *et al* [14] found that at zero frequency, AHC (σ_{xy}) in bcc Fe, fcc Ni, and hcp Co is 753, −2203, and 477 $(\Omega\ \mathrm{cm})^{-1}$, respectively. Bianco *et al* [15] calculated the AHC in Fe_3Co, and the σ_{xy} value at zero frequency is 452 $(\Omega\ \mathrm{cm})^{-1}$. Huang *et al* [16] calculated the AHC of the Heusler compound such as Co_2FeAl and found it to be 39 $(\Omega\ \mathrm{cm})^{-1}$.

While σ_{xy} originates from magnetism, the proportionality coefficient between σ_{xy} and the magnetic moment is difficult to predict without performing an explicit first-principles calculation. As discussed in early work on frequency dependence of σ_{xy} from [9], as well as in later [13–15, 17], different parts of the reciprocal space can have either positive or negative contribution to σ_{xy}, as sign will in general depend on position of the Fermi level relative to the subtle spin–orbit induced band gaps in the band-structure. Therefore, we might expect that, generally σ_{xy} will be a very sensitive function of the electronic band structure. As a consequence, we expect a rich dependence of dynamic $\sigma_{xy}(\omega)$ in the low-frequency range. In particular, we expect that there will be a strong frequency dependence of $\sigma_{xy}(\omega)$ when $\hbar\omega$ is close to the energy of the spin–orbit split bands in the band structure. The energy of the spin–orbit split bands is on the order of tens of meV in ferromagnetic metals such as Fe, Co, or Ni. These energies lie in the range of frequencies ∼10 THz, within the so-called *terahertz-gap*: the range of frequencies in the electromagnetic spectrum that are in between the microwave radio frequencies and optical frequencies.

Moreover, we quite generally expect that σ_{xy} will be very sensitive on alloying, as even subtle changes in the electronic band structure will change the position of spin–orbit split bands relative to the Fermi level. In this study, we use first-principles techniques to calculate the $\sigma_{xy}(\omega)$ in the THz regime for a specific ternary metallic alloy system, Fe–Co–Al. We decided to focus on this alloy in particular, as it is known that the addition of Co to Fe leads to strong variations of spin-polarized density of states, as studied, for example, in [18]. Furthermore, even small addition of Al to Fe–Co can lead to large changes in the measured spin-dependent physical properties, as shown in [19–21]. Our calculations show that alloying is indeed a feasible way to change the THz optical response of ferromagnetic metals in the Fe–Co–Al ternary system. Our results show that alloys like Fe–Co–Al are promising candidates for developing magnetic optical metamaterials, where the manipulation of both magnetic moment orientation and chemical composition serves to regulate their interaction with light.

The early work from [9] focuses on the frequency dependence of σ_{xy} in Fe, Co, and Ni for frequencies ω above 24 THz (0.1 eV). Most other studies of frequency-dependent σ_{xy} are carried out in the optical regime, at even higher energies. For example, [22] computed σ_{xy} for Fe_3Co and $FeCo_3$ in the 120–1300 THz (0.5–5.2 eV) energy range. Next, [23] calculated the optical response of $Fe_{4-x}Co_x$ (with $x = 1$–3) up to the 3100 THz (13 eV) range, while [24, 25] reported σ_{xy} for FeAl in the 120–1500 THz (0.5–6 eV) range. Recently, some studies have focused on the off-diagonal optical response in the THz regime. Seifert *et al* [26] studied the off-diagonal optical response in $DyCo_5$, $Co_{0.32}Fe_{0.68}$ and $Gd_{0.27}Fe_{0.73}$, and they measured somewhat stronger dependence of σ_{xy} on ω in the range of frequencies below 10 THz. Matsuda *et al* [12] studied the off-diagonal optical response in Weyl antiferromagnet Mn_3Sn at very low energy (2.4 THz) and they find weak dependence of σ_{xy} on frequency. On the other hand, calculated and measured σ_{xy} in the THz regime is very frequency dependent in $SrRuO_3$, as shown in [27–29].

We organize the paper as follows. In section 2 we show the calculation methods. In section 3 we present and analyze our results. We conclude in section 4.

2. Methods

We use the Quantum Espresso package [30] to calculate the electronic structure of ordered alloys of Fe, Co, and Al. We use the generalized gradient approximation of Perdew *et al* [31] along with the optimized norm-conserving Vanderbilt pseudopotentials which include spin–orbit interaction [32–34]. We choose 120 Ha kinetic-energy cutoff for the plane-wave expansion of the valence wave functions. A $16 \times 16 \times 16$ Monkhorst–Pack grid and a smearing [35] of 0.01 Ry are used to sample the electron's Brillouin zone. We computed $\sigma_{xy}(\omega)$ using the standard Kubo formula [36],

$$\sigma_{\alpha\beta}(\omega) = \frac{ie^2\hbar}{VN_k} \lim_{\delta\to 0} \sum_{\mathbf{k}} \sum_{nm} \frac{f_{m\mathbf{k}} - f_{n\mathbf{k}}}{\varepsilon_{m\mathbf{k}} - \varepsilon_{n\mathbf{k}}} \frac{\langle \phi_{n\mathbf{k}} | v_\alpha | \phi_{m\mathbf{k}} \rangle \langle \phi_{m\mathbf{k}} | v_\beta | \phi_{n\mathbf{k}} \rangle}{\varepsilon_{m\mathbf{k}} - \varepsilon_{n\mathbf{k}} - \hbar\omega - i\delta/2} \tag{1}$$

that was already used successfully in [8–11]. Here, α and β denote Cartesian directions. V is the cell volume. Indices n and m denote different electronic bands. $\mathbf{k}$ represents the wave vector in the Brillouin zone. N_k is the number of k-points, and $f_{n\mathbf{k}}$ is the Fermi–Dirac distribution function. ω is the optical frequency. We use the Wannier interpolation [37, 38] in evaluating equation (1), as these calculations require a very dense sampling of the Brillouin zone. We tested the convergence of σ_{xy} with the choice of the k mesh. We use adaptive k-mesh refinement to accelerate convergence [13] by adding a $5 \times 5 \times 5$ fine mesh around regions with a large contribution to $\sigma_{xy}(\omega)$. For pure metals (Fe and Co), a $250 \times 250 \times 250$ primary k-mesh is enough to achieve the convergence of σ_{xy}. For calculations with two atoms per unit cell and four atoms per unit cell, a $200 \times 200 \times 200$ and $150 \times 150 \times 150$ k-mesh, respectively, was enough to achieve convergence.

In this work we mostly stay within the intrinsic limit $\delta \to 0$ of the σ_{xy} for small ω, as given by equation (1). For future work we leave the role of finite electron lifetime, random disorder, or temperature effects on $\sigma_{xy}(\omega)$ in the THz regime. As discussed in section 4 we attempt to approximately model disorder within the approach of [39].

To validate the reliability of our calculation approach, we compare our calculation results with previous calculations. Our calculated σ_{xy} of Fe and Co at zero frequency are 758 and 471 $(\Omega\ \mathrm{cm})^{-1}$, respectively, which agrees very well with the previous calculation result of 753 $(\Omega\ \mathrm{cm})^{-1}$ in Fe and 477 $(\Omega\ \mathrm{cm})^{-1}$ in Co [14]. Furthermore, the calculated σ_{xy} of FeCo and Fe_3Co at zero frequency is 226 and 416 $(\Omega\ \mathrm{cm})^{-1}$, respectively. The measured σ_{xy} of $Fe_{0.68}Co_{0.32}$ at zero frequency is about 350 $(\Omega\ \mathrm{cm})^{-1}$ [26], which lies between the theoretical values of FeCo and Fe_3Co. Furthermore, we calculated the Kerr angle of Fe in the range of 0–1.2 eV by using our calculated σ_{xy} values and experimental σ_{xx} values from [40, 41]. Our calculated Kerr angle matches very well with the results in [42].

In all of our calculations, we assumed that the magnetization points along the [001] direction. We did not explore what happens to the off-diagonal conductivity when the magnetization points in any other crystallographic direction, such as [011] or [111]. We decided to restrict our calculations to those with the magnetization axis pointing along the [001] direction, as our goal here is to compare σ_{xy} only as a function of the chemical composition of the alloy and frequency. Furthermore, for consistency, in each calculation we chose the same sign of magnetization along the [001] direction.

3. Results and discussion

Now we present our results for ordered Fe–Co–Al alloys. We start by discussing the computed lattice constants and crystal structure of these alloys. Our results are shown in table 1. Most of the ordered alloys we studied order in the bcc-derived structures B_2 and $D0_3$ [43–45]. The B_2 structure is a bcc-derived structure with two atoms in the primitive unit cell. This structure is therefore present in alloys with the ratio of 1–1 of two elements. On the other hand, $D0_3$ structure contains four atoms in the primitive unit cell, so it is present in ordered binary alloys with the 1–3 ratio of constituent elements, or the 1–1–2 ratio in the case of ternary alloys. Among the ordered alloys we studied, the only ones that are not in the bcc-derived structure are Al, $FeAl_3$, $CoAl_3$, Co, and Co_3Al. However, three of these (Al, $FeAl_3$, and $CoAl_3$) are nonmagnetic, regardless of their crystal structure, so their σ_{xy} is identically zero. Therefore, we do not discuss these cases in more detail. Next, in the case of Co, we explicitly showed that $\sigma_{xy}(\omega)$ is very similar in bcc and hcp structures. Therefore, for a more consistent comparison with other members of the Fe–Co–Al family of compounds, we will show results for pure Co in its bcc structure. Finally, we expect that the remaining exception, Co-rich Co_3Al, will also have $\sigma_{xy}(\omega)$ that does not strongly depend on the structure, so that we are justified in studying Co_3Al in the bcc-derived structure (and not in the lowest energy structure, the fcc-derived $L1_2$).

We find that the computed lattice constants are close to the values experimentally measured. Small deviations, on the order of 1% are due to the approximations in our exchange-correlation functional, as well as thermal expansion, as the experimental data in table 1 are taken at room temperature.

Table 1. Calculated magnetic moment and lattice constant of ordered Fe–Co–Al alloys. The magnetic moment is on a per atom basis for nominally magnetic Fe and Co atoms.

		M (μ_B/atom)	a^{calc} (Å)	a^{exp} (Å)
Fe	bcc	2.26	2.84	2.86 [48]
Fe_3Co	$D0_3$	2.36	5.71	5.71 [22]
FeCo	B_2	2.30	2.85	2.85 [49]
$FeCo_3$	$D0_3$	2.02	5.66	5.66 [22]
Co	bcc	1.80	2.82	2.82 [50]
Co	hcp	1.62	$a = 2.50$	$a = 2.50$
			$c = 4.04$	$c = 4.09$ [48]
Fe_3Al	$D0_3$	1.55	5.76	5.79 [51]
FeAl	B_2	0.36	2.88	2.91 [52]
$FeAl_3$	$D0_3$	.	5.98	
Co_3Al	$D0_3$	1.05	5.69	
CoAl	B_2	.	2.86	2.86 [53]
$CoAl_3$	$D0_3$	.	6.01	
Fe_2CoAl	$D0_3$	1.54	5.76	5.73 [54]
$FeCo_2Al$	$D0_3$	1.25	5.71	5.73 [55]

Calculated magnetic moments per atom are also given in table 1. Most of these ordered alloys are magnetic in our calculations, with the exception of Al-rich compounds, such as $FeAl_3$, $CoAl_3$ and CoAl. These findings are in agreement with previous studies [46, 47].

3.1. Fe and Co

Figure 1 shows calculated $\sigma_{xy}(\omega)$ of pure Fe and Co metal in the range of energies from $\hbar\omega \sim 0$–0.1 eV. This corresponds to the range of frequencies $\omega/(2\pi) \sim 0$–25 THz. As expected, we find a strong variation of $\sigma_{xy}(\omega)$ as a function of frequency, in both Fe and Co. These variations are the strongest around 10–15 THz. We attribute these modifications to the fact that the characteristic spin–orbit gaps in these metals occur in the same range of energies. For Fe, we find that the minimal value of σ_{xy}, in the studied frequency range, is 634 $(\Omega\ \mathrm{cm})^{-1}$ at 14.5 THz, while the maximal value is 1.5 times larger, 950 $(\Omega\ \mathrm{cm})^{-1}$ at a nearby frequency of 16 THz. In the case of Co, the minimal value is 233 $(\Omega\ \mathrm{cm})^{-1}$ at 17 THz, and maximal value is 2.5 times larger, 582 $(\Omega\ \mathrm{cm})^{-1}$ at 10 THz. We compared $\sigma_{xy}(\omega)$ in bcc and hcp structure of Co and we found qualitatively similar responses, as shown in figure 1. Therefore, at least in the case of Co, the crystalline structure does not have a strong effect on $\sigma_{xy}(\omega)$.

3.2. Fe–Co alloys

After analyzing σ_{xy} in pure Fe and Co, we now turn to the ordered Fe–Co alloys. We considered three ordered alloys of Fe and Co, these are Fe_3Co, FeCo, and $FeCo_3$. The ordered crystalline structures of these alloys are bcc-derived $D0_3$, B_2 and $D0_3$, respectively. Our results for Fe–Co alloys are shown in figure 2. Starting from pure Fe, we find that the addition of Co at first significantly reduces the value of σ_{xy}. In particular,

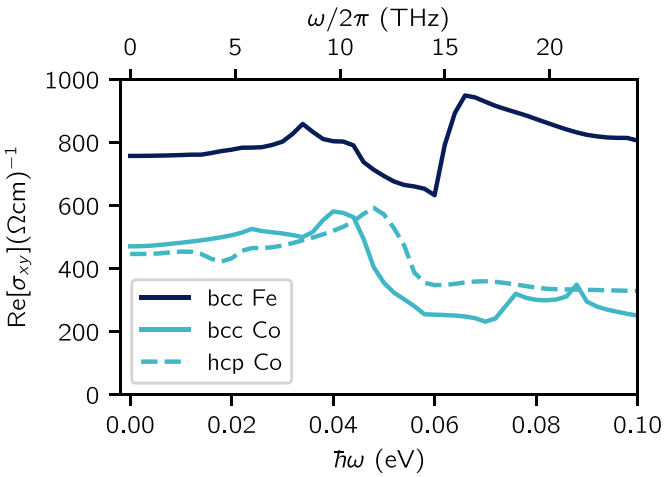

Figure 1. Calculated real part of σ_{xy} for bcc Fe, bcc Co, and hcp Co as a function of ω.

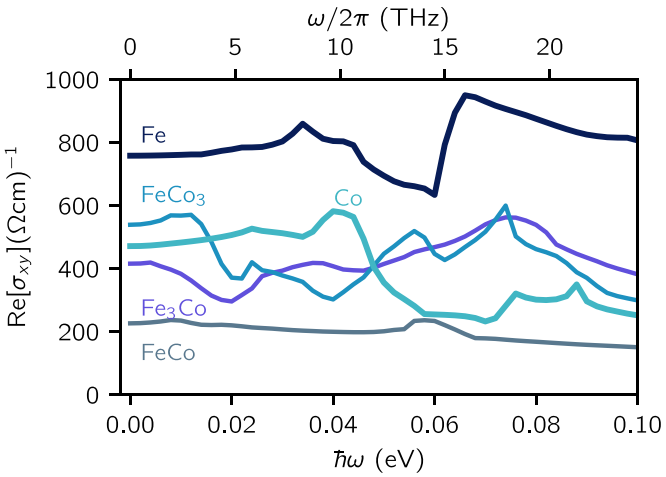

Figure 2. Calculated real part of σ_{xy} for bcc Fe, $D0_3$ Fe_3Co, B_2 FeCo, $D0_3$ $FeCo_3$ and bcc Co as a function of ω.

σ_{xy} in Fe_3Co is on average about 2 times lower than that of pure Fe. Furthermore, the spectral features of alloy Fe_3Co are distinct from that of pure Fe. While both Fe and Co have a nearly constant σ_{xy} up to 10 THz, we find that Fe_3Co shows a strong dependence on frequency starting already around 3 THz. This finding of a large sensitivity of σ_{xy} to the chemical composition is in agreement with our expectation that σ_{xy} is very sensitive to details of the band structure. Adding even more Co, as in FeCo, we find that the value of σ_{xy} is reduced even further. In particular, σ_{xy} is about 4 times smaller in FeCo than in pure Fe. Moreover, the spectral features of FeCo are surprisingly constant in the entire range of frequencies we studied. The further addition of Co increases the value of σ_{xy}. For example, in the case of $FeCo_3$, σ_{xy} is similar in magnitude to that of pure Co. The spectral features of $FeCo_3$ are the strongest among the Fe–Co alloys we studied.

The nonmonotonic dependence of σ_{xy} on Co concentration is reminiscent of a nonmonotonic dependence of magnetic damping observed in Fe–Co alloys [18]. Although magnetic damping is not directly related to σ_{xy}, we expect that both can

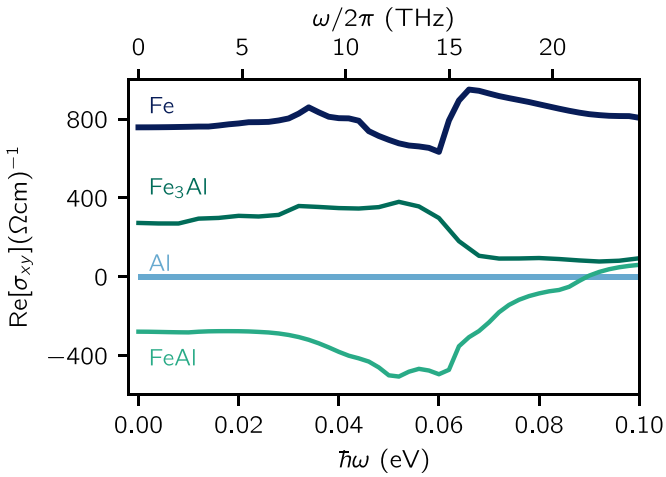

Figure 3. Calculated real part of σ_{xy} for bcc Fe, $D0_3$ Fe_3Al, B_2 FeAl and bcc Al as a function of ω.

be related to changes in the nature of the electronic band structure near the Fermi level in Fe–Co alloys.

We note that variation in σ_{xy} on Co concentration cannot be rationalized with variation of the magnetic moment, as we find that all members of the Fe–Co family of alloys have nearly constant magnetic moment per atom, on the order of $\sim 2\ \mu_B$ (see table 1). Therefore, even though σ_{xy} can be used as a magnetic order signature, one is not necessarily proportional to the other. As discussed earlier, the role of the magnetic order here is only to break the time-reversal symmetry, while the magnitude and spectral properties of σ_{xy} are driven by the spin–orbit interaction of electron bands close to the Fermi level.

Comparing the band structure of all Fe–Co ordered alloys we studied, we find that the overall band structure has not changed much, but only the position of the Fermi level relative to the rigid band structure is increasing with the addition of Co. Therefore, we attribute the changes in the σ_{xy} of Fe–Co alloys to changes in the relative position of the Fermi level, and not to changes in the band structure itself.

3.3. *Fe–Al alloys*

Next, we discuss the calculated σ_{xy} in Fe–Al alloys. Our results are shown in figure 3. Since Al is non-magnetic, the σ_{xy} response is, by symmetry, zero at all frequencies. When Al is introduced, the σ_{xy} response of Fe_3Al lies between that of pure Fe and Al, as expected. However, unexpectedly, when the Al concentration reaches 50%, σ_{xy} response of FeAl changes sign in the entire frequency range from 0 to 20 THz. We ensured that, in all of these cases, the Fe and Fe–Al alloys have magnetization pointing in the same direction. A similar result is observed in Co/Pd multi-layers in [56], where the sign of σ_{xy} changes depending on the relative concentration of Co to Pd.

3.4. *Co–Al alloys*

The next binary alloys we discuss are Co–Al alloys. Results for these alloys are shown in figure 4. Our calculations find that CoAl and $CoAl_3$ are not magnetic while the Co-rich compound

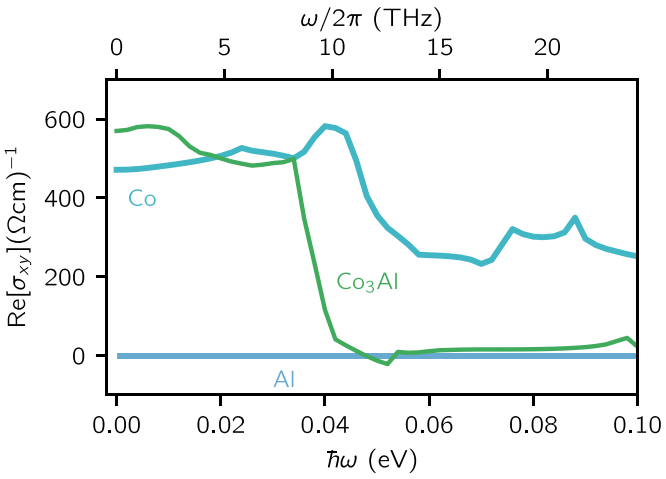

Figure 4. Calculated real part of σ_{xy} for bcc Co, $D0_3$ Co_3Al and bcc Al as a function of ω.

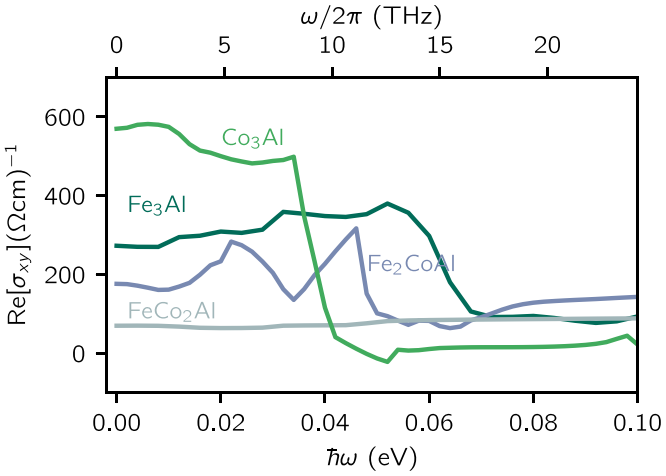

Figure 5. Calculated real part of σ_{xy} for $D0_3$ Fe_3Al, $D0_3$ Fe_2CoAl, $D0_3$ $FeCo_2Al$ and $D0_3$ Co_3Al as a function of ω.

Co_3Al is magnetic. At low frequencies, below 10 THz, we find that σ_{xy} for Co_3Al is quite large, and somewhat constant, with the value of $\sim$500 $(\Omega\ \mathrm{cm})^{-1}$. However, above 10 THz, σ_{xy} is reduced 50-fold to only $\sim$10 $(\Omega\ \mathrm{cm})^{-1}$.

3.5. Fe–Co–Al ternary alloys

So far, we discussed the σ_{xy} response of binary alloys. In what follows, we consider several Fe–Co–Al ternary alloys. We kept the Al concentration at 25%, and varied the relative concentration of Fe and Co. The results for these alloys are shown in figure 5. The behavior of Fe_2CoAl is qualitatively similar to that of Fe_3Al, so the replacement of Fe with Co did not change qualitatively $\sigma_{xy}(\omega)$. Quantitatively, we find that σ_{xy} is approximately $\sim$1.5 times lower in Fe_2CoAl relative to Fe_3Al. However, with an even higher concentration of Co, as in $FeCo_2Al$, we find $\sigma_{xy}(\omega)$ which is qualitatively and quantitatively different from other members of the Fe–Co–Al family of compounds. In particular, we find an unusually small σ_{xy}

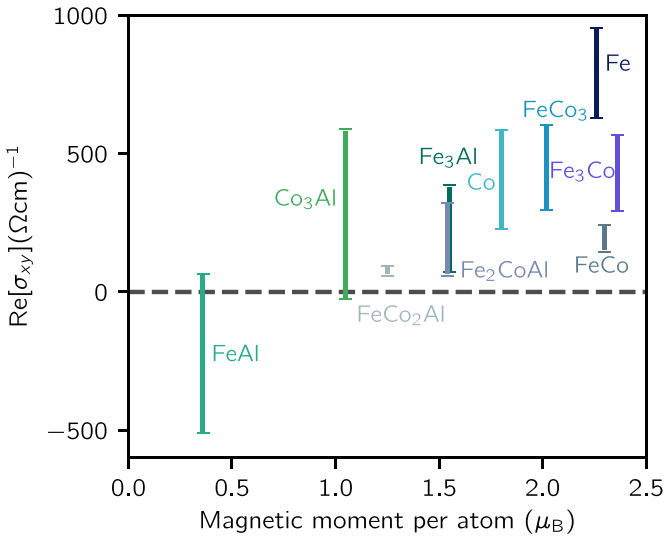

Figure 6. The summary of σ_{xy} in the range of 0.0–0.1 eV and magnetic moment per atom of each metal and alloy. The bar shows the maximum and minimum of the σ_{xy} in the range of 0.0–0.1 eV.

in $FeCo_2Al$, around 80 $(\Omega\ \mathrm{cm})^{-1}$, that is almost insensitive to the frequency ω in the entire range between 0 and 25 THz.

3.6. Optical conductivity and magnetic moment

As we discussed earlier, σ_{xy} is often taken as an optical signature of magnetic order. Therefore, it is natural to ask whether a material with a large magnetization will also have a large σ_{xy}. Figure 6 shows the relationship between σ_{xy} and the magnetic moment per atom for all of the compounds we studied. For each compound we show on the vertical scale of figure 6 the range of maximal and minimal values of the calculated σ_{xy} in the range of frequencies from 0 to 25 THz. As can be seen from the figure, we find that in the case of Fe–Co alloys, the magnetic moments per atom are nearly the same, on the order of $\sim$2 μ_B, but the σ_{xy} ranges from 150, all the way to 950 $(\Omega\ \mathrm{cm})^{-1}$. The same is true for the other compounds we studied. The most drastic example is FeAl in which σ_{xy} even changes sign relative to that of Fe. Therefore we can conclude that materials with larger magnetic moment do not necessarily have larger σ_{xy}. This is not too surprising, as the large magnetization arises from the large difference in population of dominantly spin-up and spin-down bands. However, a large σ_{xy} in the low-frequency regime relies on detailed information about spin orbit split bands near the Fermi level.

3.7. Imaginary part of the off-diagonal component σ_{xy}

So far we have focused on the frequency dependence of the real part of σ_{xy} in Fe–Co–Al ternary system. However, there are other changes to the conductivity tensor induced by the magnetic order. These are the imaginary part of the off-diagonal component σ_{xy}, as well as the difference between the diagonal components of the conductivity tensor along and perpendicular to the direction of the magnetic moment, $\sigma_{zz} - \sigma_{xx}$.

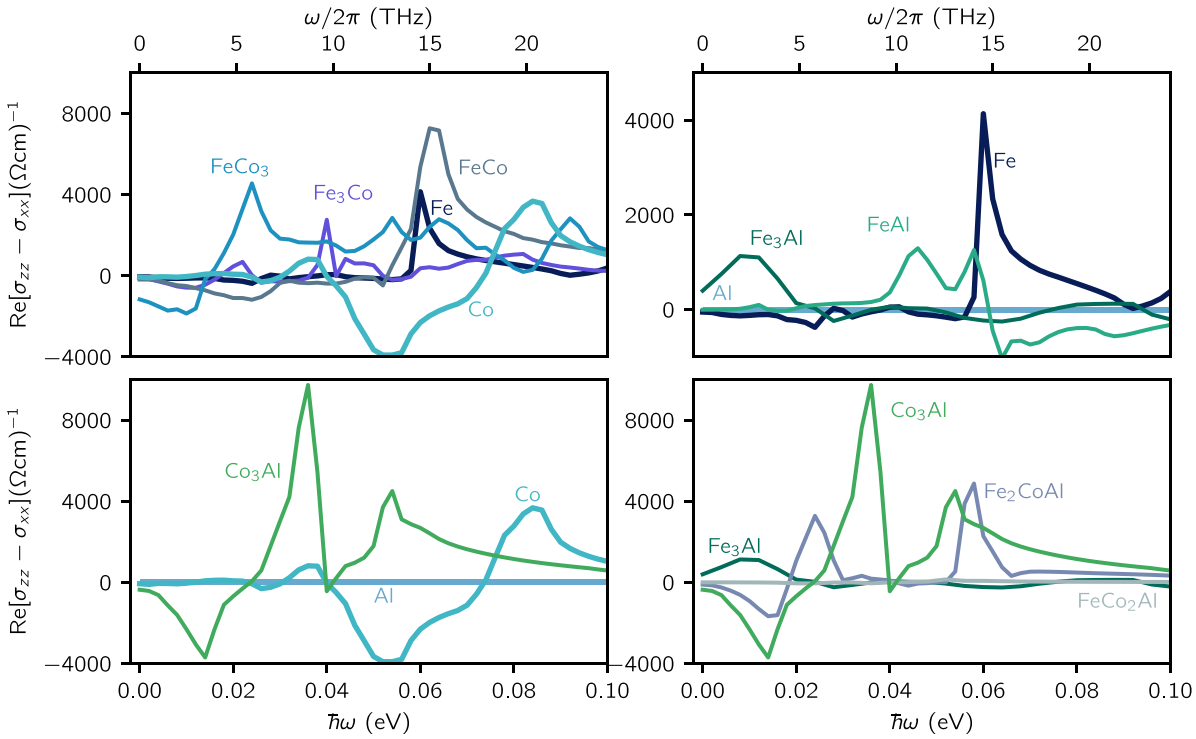

Figure 7. Calculated real part of σ_{zz}–σ_{xx} for Fe–Co–Al metals and alloys as a function of frequency ω.

We first briefly discuss the imaginary part of σ_{xy} which contributes to the MOKE in addition to the real part of σ_{xy}. The imaginary part of σ_{xy} is shown in the supplement for all the compounds we studied. As expected from the Kramers–Kronig relationship, the imaginary part of σ_{xy} is also strongly dependent on both chemical composition and frequency. For example, we find that the step-like spectral feature we found for the real part of σ_{xy} in Co_3Al is accompanied with a single sharp feature in the imaginary part of σ_{xy}, at nearly the same frequency (∼10 THz), as one might expect. Similarly, sharp features in the imaginary part of σ_{xy} we find in the case of Co and Fe_3Al. The spectral features of the imaginary part of σ_{xy} are much more complex for the other compounds we studied. This is particularly true for alloys containing Fe magnetic atoms.

3.8. $\sigma_{zz} - \sigma_{xx}$

For completeness, we now analyze the remaining component of the conductivity tensor that depends on the presence of the magnetic order. By symmetry, magnetization along the z axis introduces a spin–orbit driven difference between the σ_{zz} (along the magnetization axis) and $\sigma_{xx} = \sigma_{yy}$ (perpendicular to the magnetization axis). While the difference $\sigma_{zz} - \sigma_{xx}$ does not contribute to the MOKE it does contribute to the second order change in the birefringence (Voigt effect). While σ_{xy} is zero without magnetic order, the diagonal components $\sigma_{xx} = \sigma_{yy}$ and σ_{zz} are not. Therefore, here we do not focus on these diagonal components individually, but instead we focus on their difference, $\sigma_{zz} - \sigma_{xx}$. The calculated values of $\sigma_{zz} - \sigma_{xx}$ for all compounds we studied are shown in figure 7.

Again, we find strong variations of $\sigma_{zz} - \sigma_{xx}$ both as a function of frequency and as a function of chemical composition. In the case of the Fe–Co family of compounds, we find that $\sigma_{zz} - \sigma_{xx}$ in Fe and FeCo have a sharp peak around 15 THz, and are nearly zero below 14 THz. Co shows two sharp features, with opposite signs, one at around 9 and another around 20 THz. The addition of 25% of Al to Fe strongly changes the value of $\sigma_{zz} - \sigma_{xx}$. While Fe has a sharp feature around 15 THz, Fe_3Al has a sharp feature around 3 THz. The addition of even more Al, as in FeAl, introduces two sharp features, at around 10 and 15 THz. The addition of Al to Co also introduces significant qualitative and quantitative changes to $\sigma_{zz} - \sigma_{xx}$.

4. Discussion and conclusion

We find a strong dependence of $\sigma_{xy}(\omega)$ in the terahertz frequency range for Fe–Co–Al ordered alloys. For example, in the case of Co_3Al we find a nearly 50-fold reduction in $\sigma_{xy}(\omega)$ above 10 THz as compared to $\sigma_{xy}(\omega)$ below 10 THz. On the other hand, in the case of $FeCo_2Al$ we find a nearly constant $\sigma_{xy}(\omega)$ in the entire range from 0 to 25 THz. Furthermore, we also find a strong dependence of $\sigma_{xy}(\omega)$ on the chemical composition. For example, the addition of Al to Fe can change the sign of $\sigma_{xy}(\omega)$, so that $\sigma_{xy}(\omega)$ is positive in Fe and Fe_3Al but negative in the case of FeAl. Similarly, the addition of Co to Fe produces a nonmonotonic dependence of $\sigma_{xy}(\omega)$ on Co concentration. As an example, $\sigma_{xy}(\omega)$ in FeCo is about 4 times smaller than in Fe and 3 times smaller than that in Co.

We attribute both of these strong variations, with frequency and composition, to the changes in the electronic structure

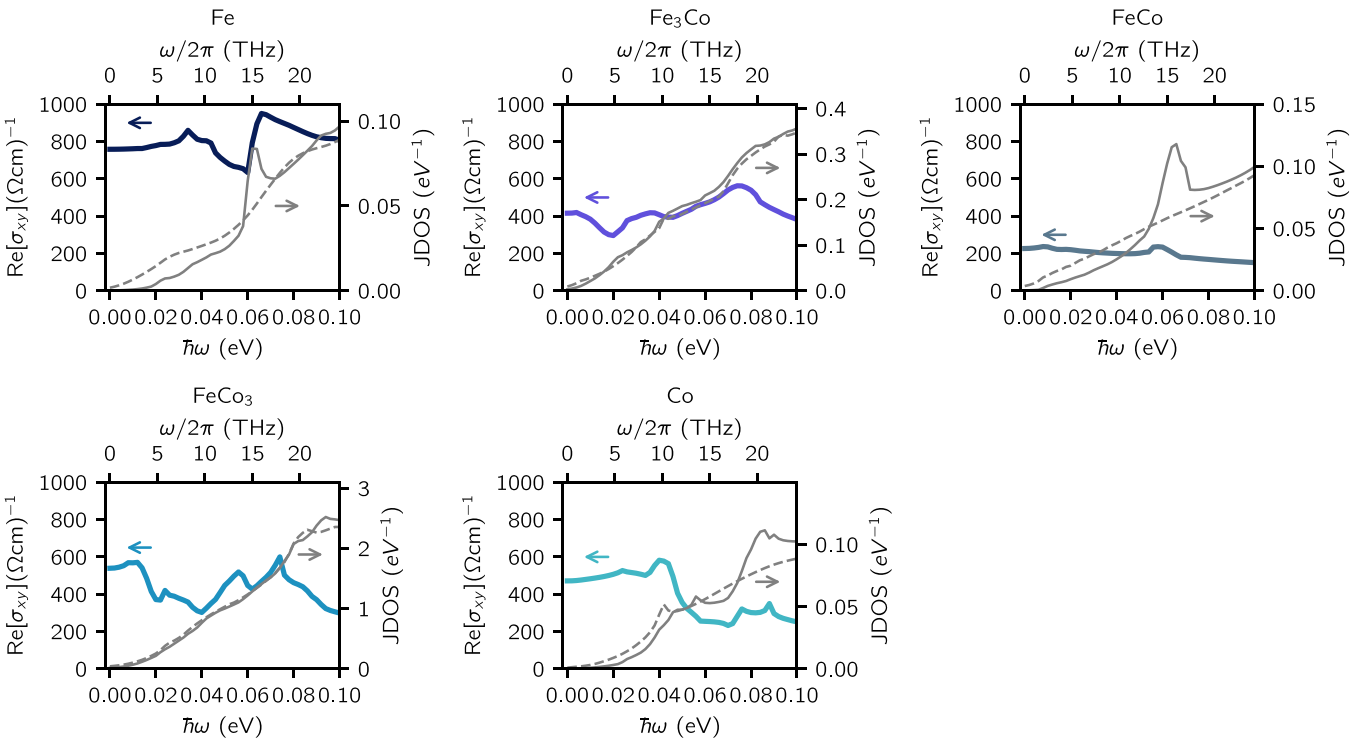

Figure 8. Calculated joint density of states of Fe–Co alloys as a function of frequency ω. The grey lines show the density of states with the spin–orbit coupling (solid gray line) and without the spin–orbit coupling (dashed gray line). Spectral features present in the solid gray line, but not in the dashed gray line, can therefore be assigned to the presence of the spin–orbit interaction. The colored lines show the real part of σ_{xy} in the same frequency range as the joint density of states.

induced by the presence of the spin–orbit interaction. Detailed, k-space resolved, analysis of $\sigma_{xy}(\omega)$ is rather involved, even in the case of pure Fe, at $\omega = 0$. For example, [17] found that the $\sigma_{xy}(\omega = 0)$ of pure Fe is contributed both by small regions of k-space, close to avoided crossings, which contribute to the AHE with high intensity, and equally important, background contributions with smaller intensity, but present at nearly all k-points. The analysis is additionally complicated in our work, as we study binary and ternary alloys, and we study $\omega > 0$ which cannot be written as a sum over the occupied states. Therefore, we leave a more detailed analysis of the origin of these strong variations of $\sigma_{xy}(\omega)$ to future studies.

Instead, here we focus on a different analysis, inspired by the findings of [17]. Our analysis is based on the joint density of states (JDOS). Such an analysis sums over all k points and can therefore be equally well applied to pure metals as well as to alloys, regardless of the number of atoms in the primitive unit cell. Furthermore, this analysis is particularly well suited for analysis of σ_{xy} at nonzero frequencies ω, since JDOS counts how many states are available for transition at a particular frequency ω.

We start our analysis by first computing JDOS without including spin–orbit interaction in the calculation. Next, we include spin–orbit interaction in the calculation, and compute the JDOS once again. Comparing the JDOS between those two calculations tells us what is the effect of the spin orbit on the electronic spectrum. Clearly, any changes in the electronic spectrum induced by spin–orbit interaction should correlate with σ_{xy}, as σ_{xy} originates purely from the spin–orbit interaction. We then expect that the frequencies ω where the two JDOS differ will reflect in $\sigma_{xy}(\omega)$, as this is the part of the spectrum where the spin–orbit interaction has redistributed the weight of electronic states. We report the JDOS with and without inclusion of the spin–orbit interaction in figures 8–11. Dashed gray lines show JDOS without spin–orbit interaction, whereas solid gray lines show JDOS with spin–orbit interaction. As can be seen in the figures, we find that whenever $\sigma_{xy}(\omega)$ experiences a large change as a function of ω, there is a corresponding spike in the JDOS due to the inclusion of the spin–orbit interaction. Therefore, the gaps in the electron spectrum induced by the spin–orbit interaction are well correlated to $\sigma_{xy}(\omega)$, as expected.

Our calculations are performed in the limit of infinite electron lifetime. While this is justified for materials with moderate amount of disorder, with diagonal conductivity around 10^4–10^6 $(\Omega\ \mathrm{cm})^{-1}$, we leave for future work discussion of role of disorder on $\sigma_{xy}(\omega)$ in the terahertz range for materials that are not within the moderate range of disorder. We expect that at low enough frequencies the phenomenology of $\sigma_{xy}(\omega)$ will be the same as that of $\sigma_{xy}(\omega = 0)$, so that with a moderate amount of disorder the dominant contribution to $\sigma_{xy}(\omega)$ is intrinsic, but with less disorder scattering from impurities start to dominate [1]. We show in supplement $\sigma_{xy}(\omega)$ with approximately incorporated effect of the finite carrier lifetime. While the finite carrier lifetime approximation washes out some of the spectral features in $\sigma_{xy}(\omega)$, we still find that many qualitative characteristics remain, such as the change in sign of σ_{xy} near 20 THz, or the sharp decline in σ_{xy} in Co_3Al around

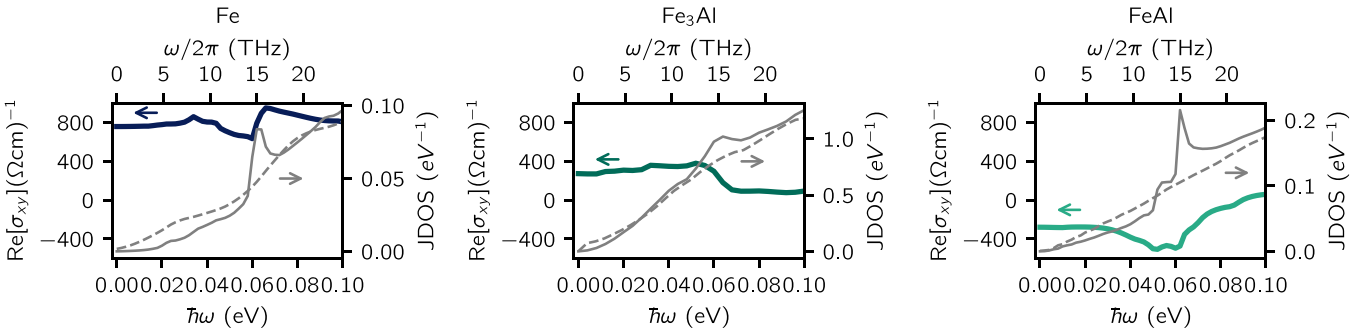

Figure 9. Calculated joint density of states of Fe–Al as a function of frequency ω. All conventions are the same as in figure 8.

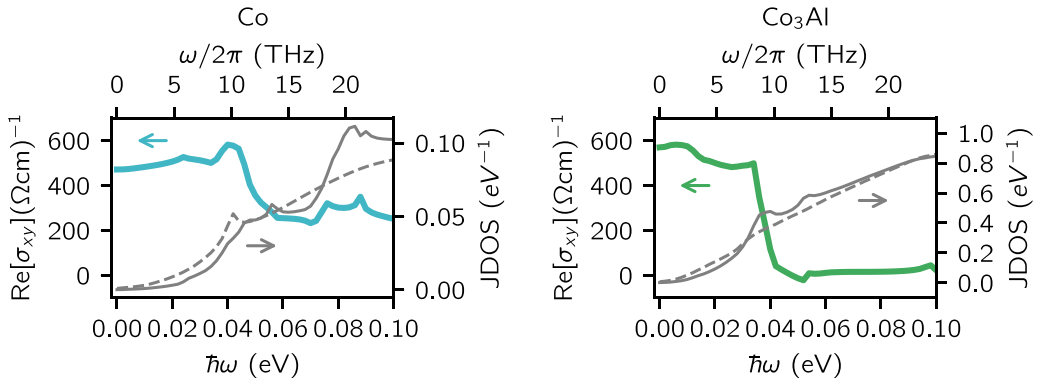

Figure 10. Calculated joint density of states of Co–Al as a function of frequency ω. All conventions are the same as in figure 8.

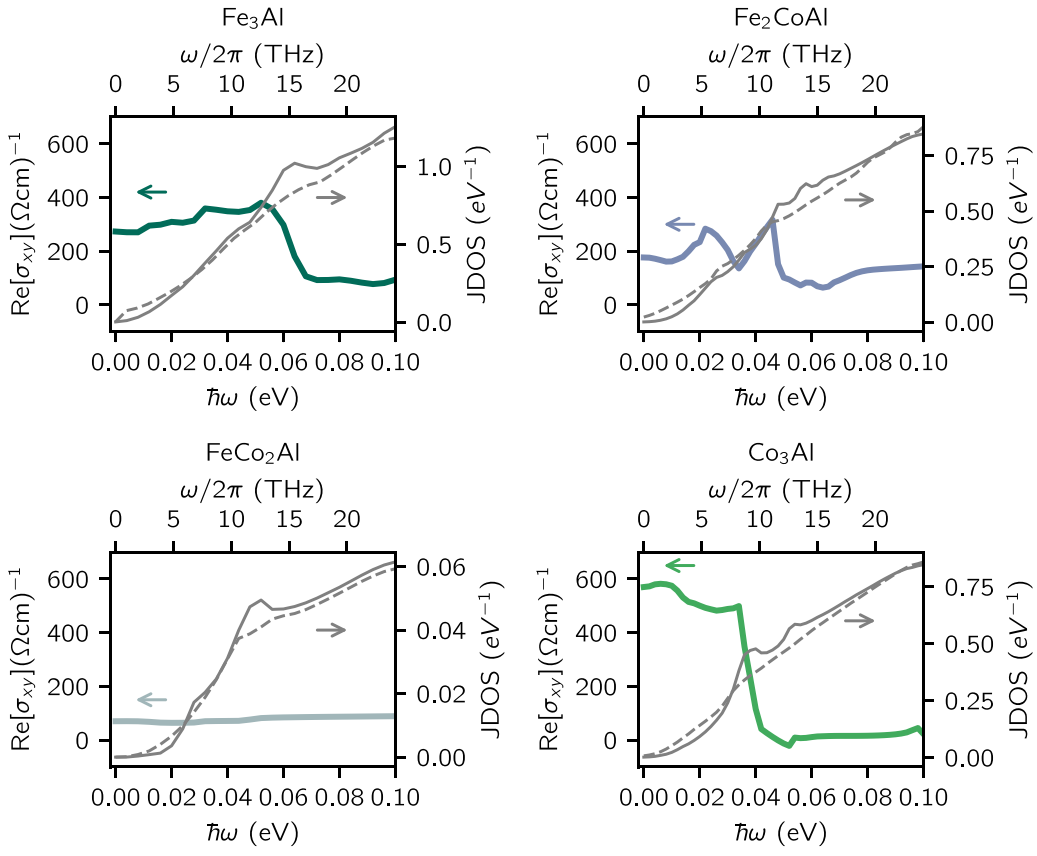

Figure 11. Calculated joint density of states of Fe–Co–Al alloys as a function of frequency ω. All conventions are the same as in figure 8.

10 THz, or non-monotonic dependence of σ_{xy} of Co concentration in Fe–Co alloys.

Our findings indicate that alloys such as Fe–Co–Al would be of interest in the creation of magnetic optical metamaterials in which the direction of magnetic moment and chemical composition are used to control its interaction with light.

Data availability statement

All data that support the findings of this study are included within the article (and any supplementary files).

Acknowledgments

This work was supported by Grant NSF DMR-1848074. Computations were performed using the HPCC computer cluster at UCR. We acknowledge discussion with Igor Barsukov and Richard B Wilson.

ORCID iD

Ming Lei https://orcid.org/0000-0001-6015-0762

References

[1] Nagaosa N, Sinova J, Shigeki Onoda A H M and Ong N P 2010 Anomalous hall effect *Rev. Mod. Phys.* **82** 1539–92
[2] John K 1877 XLIII on rotation of the plane of polarization by reflection from the pole of a magnet *London, Edinburgh Dublin Phil. Mag.* **3** 321–43
[3] Mark H K 1985 Magneto-optic recording technology (invited) *J. Appl. Phys.* **57** 3913–8
[4] Meiklejohn W H 1986 Magnetooptics: a thermomagnetic recording technology *Proc. IEEE* **74** 1570–81
[5] Atmatzakis E, Papasimakis N, Fedotov V and Zheludev N I 2014 Giant kerr rotation enhancement in magneto-plasmonic metamaterials *CLEO: 2014* (Optical Society of America) p STu1H.6
[6] Wang X, Wang H, Jian J, Rutherford B X, Gao X, Xiaoshan X, Zhang X and Wang H 2020 Metal-free oxide-nitride heterostructure as a tunable hyperbolic metamaterial platform *Nano Lett.* **20** 6614–22
[7] Haldane F D M 2004 Berry curvature on the fermi surface: Anomalous hall effect as a topological fermi-liquid property *Phys. Rev. Lett.* **93** 206602
[8] Wang C S and Callaway J 1974 Band structure of nickel: spin-orbit coupling, the fermi surface and the optical conductivity *Phys. Rev.* B **9** 4897–907
[9] Uspenskii Y and Khalilov S V 1989 Electron structure and magneto-optics of ferromagnetic 3d-metals *Zh. Eksp. Teor. Fiz.* **95** 1022–36
[10] Oppeneer P M, Maurer T, Sticht J and Kübler J 1992 Ab initio calculated magneto-optical kerr effect of ferromagnetic metals: Fe and Ni *Phys. Rev.* B **45** 10924–33
[11] Guo G Y and Ebert H 1995 Band-theoretical investigation of the magneto-optical kerr effect in Fe and Co multilayers *Phys. Rev.* B **51** 12633–43
[12] Matsuda T, Kanda N, Higo T, Armitage N P, Nakatsuji S and Matsunaga R 2020 Room-temperature terahertz anomalous hall effect in weyl antiferromagnet Mn3sn thin films *Nat. Commun.* **11** 909
[13] Yao Y, Leonard Kleinman A H M, Jairo Sinova T J, Wang D-sheng, Wang E and Niu Q 2004 First principles calculation of anomalous hall conductivity in ferromagnetic bcc Fe *Phys. Rev. Lett.* **92** 037204
[14] Wang X, Vanderbilt D, Yates J R and Souza I 2007 Fermi-surface calculation of the anomalous hall conductivity *Phys. Rev.* B **76** 195109
[15] Bianco R, Resta R and Souza I 2014 How disorder affects the berry-phase anomalous hall conductivity: a reciprocal-space analysis *Phys. Rev.* B **90** 125153
[16] Huang H-L, Tung J-C and Guo G-Y 2015 Anomalous hall effect and current spin polarization in Co_2FeX Heusler compounds (X= Al, Ga, In, Si, Ge, and Sn): a systematic ab initio study *Phys. Rev.* B **91** 134409
[17] Wang X, Yates J R, Souza I and Vanderbilt D 2006 Ab initio calculation of the anomalous hall conductivity by wannier interpolation *Phys. Rev.* B **74** 195118
[18] Schoen M A W, Thonig D, Schneider M L, Silva T J, Nembach H T, Eriksson O, Karis O and Shaw J M 2016 Ultra-low magnetic damping of a metallic ferromagnet *Nat. Phys.* **12** 839–42
[19] Wurmehl S, Jacobs P J, Kohlhepp J T, Swagten H J M, Koopmans B, Maat S, Carey M J and Childress J R 2011 Local formation of a Heusler structure in CoFe-Al alloys *Appl. Phys. Lett.* **98** 012506
[20] Bridoux G, Costache M V, Van de Vondel J, Neumann I and Valenzuela S O 2011 Enhanced spin signal in nonlocal devices based on a ferromagnetic CoFeAl alloy *Appl. Phys. Lett.* **99** 102107
[21] Shaojie H, Itoh H and Kimura T 2014 Efficient thermal spin injection using cofeal nanowire *NPG Asia Mater.* **6** e127–127
[22] Kim K J, Lee S J and Park J M 2002 Electronic structure of DO3-ordered Fe_3Co and Co_3Fe studied by spectroscopic ellipsometry *J. Magn. Magn. Mater.* **241** 6–10
[23] Kumar M, Nautiyal T and Auluck S 2010 Optical and magneto-optical properties of $Fe_{4-x}Co_x$(x = 1–3) *Eur. Phys. J.* B **73** 423–32
[24] Yull Rhee J 2004 Optical properties of correlation-induced paramagnetic feal alloy *J. Appl. Phys.* **96** 7018–21
[25] Adebambo P O, Bamgbose K M, Olowofela J A Oguntuase J A and Adebayo G A 2010 Electronic structure and optical properties of alpha-Fe-Al alloy from ab initio calculations *Physica* B **405** 4578–81
[26] Seifert T S *et al* 2021 Frequency-independent terahertz anomalous hall effect in dyco5, co32fe68 and gd27fe73 thin films from dc to 40 thz *Adv. Mater.* **33** 2007398
[27] Kim M-H, Acbas G, Yang M-H, Eginligil M, Khalifah P, Ohkubo I, Christen H, Mandrus D, Fang Z and Cerne J 2010 Infrared anomalous hall effect in $SrRuO_3$: Exploring evidence for crossover to intrinsic behavior *Phys. Rev.* B **81** 235218
[28] Fang Z, Nagaosa N, Takahashi K S, Asamitsu A, Mathieu R, Ogasawara T, Yamada H, Kawasaki M, Tokura Y and Terakura K 2003 The anomalous hall effect and magnetic monopoles in momentum space *Science* **302** 92–95
[29] Shimano R, Ikebe Y, Takahashi K S, Kawasaki M, Nagaosa N and Tokura Y 2011 Terahertz Faraday rotation induced by an anomalous hall effect in the itinerant ferromagnet $SrRuO_3$ *Europhys. Lett.* **95** 17002
[30] Giannozzi P *et al* 2009 QUANTUM ESPRESSO: a modular and open-source software project for quantum simulations of materials *J. Phys.: Condens. Matter* **21** 395502
[31] Perdew J P, Burke K and Ernzerhof M 1996 Generalized gradient approximation made simple *Phys. Rev. Lett.* **77** 3865–8
[32] Hamann D R 2013 Optimized norm-conserving vanderbilt pseudopotentials *Phys. Rev.* B **88** 085117
[33] Schlipf M and Gygi F 2015 Optimization algorithm for the generation of oncv pseudopotentials *Comput. Phys. Commun.* **196** 36–44

[34] Dal Corso A and Mosca Conte A 2005 Spin-orbit coupling with ultrasoft pseudopotentials: application to au and pt *Phys. Rev.* B **71** 115106
[35] Marzari N, Vanderbilt D, De Vita A and Payne M C 1999 Thermal contraction and disordering of the Al(110) surface *Phys. Rev. Lett.* **82** 3296–9
[36] Kubo R 1957 Statistical-mechanical theory of irreversible processes. I. General theory and simple applications to magnetic and conduction problems *J. Phys. Soc. Japan* **12** 570–86
[37] Marzari N, Mostofi A A, Yates J R, Souza I and Vanderbilt D 2012 Maximally localized Wannier functions: theory and applications *Rev. Mod. Phys.* **84** 1419–75
[38] Mostofi A A, Yates J R, Lee Y-S, Souza I, Vanderbilt D and Marzari N 2008 wannier90: A tool for obtaining maximally-localised Wannier functions *Comput. Phys. Commun.* **178** 685–99
[39] Cazzaniga M, Caramella L, Manini N and Onida G 2010 Ab initio intraband contributions to the optical properties of metals *Phys. Rev.* B **82** 035104
[40] Krinchik G S 1964 Magneto-optics of ferromagnetic metals *Izv. Akad. Nauk SSSR Ser. Fiz* **28** 481
[41] Ordal M A, Long L L, Bell R J, Bell R R Bell S E, Alexander R W and Ward C A 1983 Optical properties of the metals Al, Co, Cu, Au, Fe, Pb, Ni, Pd, Pt, Ag, Ti, and W in the infrared and far infrared *Appl. Opt.* **22** 1099–119
[42] Krinchik G S and Artem'ev V A 1968 Magneto-optical properties of Ni, Co and Fe in the ultraviolet, visible and infrared parts of the spectrum *Sov. Phys. JETP* **26** 1080–5
[43] Popova A N 2012 Synthesis and characterization of iron-cobalt nanoparticles *J. Phys.: Conf. Ser.* **345** 012030
[44] Ikeda O, Kainuma R, Ohnuma I, Fukamichi K and Ishida K 2002 Phase equilibria and stability of ordered b.c.c. phases in the Fe-rich portion of the Fe-Ga system *J. Alloys Compd.* **347** 198–205
[45] Okamoto H 2016 Supplemental literature review of binary phase diagrams: Ag-Yb, Al-Co, Al-I, Co-Cr, Cs-Te, In-Sr, Mg-Tl, Mn-Pd, Mo-O, Mo-Re, Ni-Os, and V-Zr *J. Phase Equilib. Diffus.* **37** 726–37
[46] Gonzales-Ormeño P G, Helena M P and Schön C G 2002 Ab-initio calculations of the formation energies of bcc-based superlattices in the Fe-Al system *Calphad* **26** 573–82
[47] Parsons D, Sucksmith W and Thompson J E 1958 The magnetization of cobalt-aluminium, cobalt-silicon, iron-aluminium and iron-silicon alloys *Phil. Mag.* A **3** 1174–84
[48] Zhu L, Soto-Medina S, Hennig R G and Manuel M V 2020 Experimental investigation of the al-co-fe phase diagram over the whole composition range *J. Alloys Compd.* **815** 152110
[49] Ellis W C 1941 Equilibrium relations the solid state of the iron-cobalt system *Trans. Am. soc. Metals* **29** 415–34
[50] Prinz G A 1985 Stabilization of bcc Co via epitaxial growth on gaas *Phys. Rev. Lett.* **54** 1051–4
[51] Popiel E, Tuszynski M, Zarek W and Rendecki T 1989 Investigation of feval alloys with do3 type structure by x-ray, magnetostatic and mossbauer effect methods *J. Less Common Met.* **146** 127–35
[52] Jordan J L and Deevi S C 2003 Vacancy formation and effects in feal *Intermetallics* **11** 507–28
[53] Cooper M J 1963 An investigation of the ordering of the phases coal and nial *Phil. Mag.* A **8** 805–10
[54] Ahmad A, Srimanta Mitra S K S and Das A K 2021 Structural, magnetic and magnetocaloric properties of Fe_2CoAl heusler nanoalloy *J. Magn. Magn. Mater.* **540** 168449
[55] Balke B, Wurmehl S, Fecher G H, Felser C, Alves M C M, Bernardi F and Morais J 2007 Structural characterization of the Co2FeZ (Z = Al, Si, Ga and Ge) Heusler compounds by x-ray diffraction and extended x-ray absorption fine structure spectroscopy *Appl. Phys. Lett.* **90** 172501
[56] Keskin V, Aktaş B, Schmalhorst J, Reiss G, Zhang H, Weischenberg J and Mokrousov Y 2013 Temperature and co thickness dependent sign change of the anomalous hall effect in co/pd multilayers: An experimental and theoretical study *Appl. Phys. Lett.* **102** 022416